NeuroImage 101 (2014) 138–149

Contents lists available at ScienceDirect

NeuroImage

journal homepage: www.elsevier.com/locate/ynimg

Chronic assessment of cerebral hemodynamics during rat forepaw electrical stimulation using functional ultrasound imaging

Alan Urban [a,*,1], Emilie Mace [b,1,2], Clément Brunner [a], Marc Heidmann [a], Jean Rossier [a], Gabriel Montaldo [a]

[a] Université Paris Descartes Sorbonne Paris Cité, Centre de Psychiatrie et Neurosciences, INSERM S894, Centre Hospitalier Sainte-Anne, Paris, France
[b] 1A Allée des bois de Gagny, 93340 Le Raincy, France

ARTICLE INFO

Article history:
Accepted 27 June 2014
Available online 6 July 2014

Keywords:
Neurovascular coupling
Functional imaging
Cerebral blood volume (CBV)
Thinned skull
Doppler ultrasound

ABSTRACT

Functional ultrasound imaging is a method recently developed to assess brain activity via hemodynamics in rodents. Doppler ultrasound signals allow the measurement of cerebral blood volume (CBV) and red blood cells' (RBCs') velocity in small vessels. However, this technique originally requires performing a large craniotomy that limits its use to acute experiments only. Moreover, a detailed description of the hemodynamic changes that underlie functional ultrasound imaging has not been described but is essential for a better interpretation of neuroimaging data.

To overcome the limitation of the craniotomy, we developed a dedicated thinned skull surgery for chronic imaging. This procedure did not induce brain inflammation nor neuronal death as confirmed by immunostaining. We successfully acquired both high-resolution images of the microvasculature and functional movies of the brain hemodynamics on the same animal at 0, 2, and 7 days without loss of quality. Then, we investigated the spatiotemporal evolution of the CBV hemodynamic response function (HRF) in response to sensory-evoked electrical stimulus (1 mA) ranging from 1 (200 μs) to 25 pulses (5 s). Our results indicate that CBV HRF parameters such as the peak amplitude, the time to peak, the full width at half-maximum and the spatial extent of the activated area increase with stimulus duration. Functional ultrasound imaging was sensitive enough to detect hemodynamic responses evoked by only a single pulse stimulus. We also observed that the RBC velocity during activation could be separated in two distinct speed ranges with the fastest velocities located in the upper part of the cortex and slower velocities in deeper layers. For the first time, functional ultrasound imaging demonstrates its potential to image brain activity chronically in small animals and offers new insights into the spatiotemporal evolution of cerebral hemodynamics.

Introduction

Functional imaging techniques are widely used both in humans and in animal models to identify regions of the brain involved in a sensory or cognitive task. These methods are all based on the display of physiological processes related to functional activity that can be directly detected by an electrical activity of neurons (i.e. voltage sensitive dye imaging, calcium imaging, magneto-electroencephalography) or indirectly by imaging hemodynamic changes induced by the neurovascular coupling in the vessels surrounding the activated neurons (i.e. functional magnetic resonance imaging (fMRI), positron emission tomography (PET), intrinsic optical imaging (IOI) and near infrared spectroscopy (NIRS)). All these techniques can vary by their level of temporal resolution (milliseconds to seconds), spatial resolution (microns to millimeters), degree of invasiveness to the brain (small cranial window to complete noninvasiveness) but to date none of them combine all advantages. Indeed, optical techniques provide the highest spatial resolution but are often limited to the surface of the brain. Despite recent development in photoacoustic tomography (Xiang et al., 2012) and OCT/Doppler-OCT (Chen et al., 2009; Srinivasan et al., 2010), their penetration in the brain tissue is still limited to only 1 mm.

fMRI is a method of choice to provide information in depth about the function of different brain areas in response to a stimulus (Ogawa et al., 1990) as well as neuronal pathways of information between different regions in resting state (Raichle et al., 2001). The Blood Oxygen Level Dependent (BOLD) effect is a quantitative method measuring the local concentration of deoxygenated hemoglobin. The BOLD effect is mostly recorded with the Echo Planar Imaging (EPI) sequence, a sequence able to record several image slices of the brain repetitively at a low temporal resolution (typically 3 s or less). Unfortunately, these EPI images

* Corresponding author at: INSERM U894, Centre Hospitalier Sainte-Anne Optogenetics and Brain Imaging, Centre de Psychiatrie & Neurosciences, 2 ter rue d'Alesia, 75014 Paris, France. Fax: +33 145807293.
E-mail address: alan.urban@alan-urban.fr (A. Urban).
[1] These authors contributed equally to this work.
[2] Present address: Institut de la Vision, 17 rue Moreau, 75012 Paris, France.

http://dx.doi.org/10.1016/j.neuroimage.2014.06.063

often suffer from a low spatial resolution and therefore high magnetic fields are required for reaching a spatial resolution of around 300 μm (Yu et al., 2010, 2012), which is crucial when imaging small animal brains.

If fMRI is a non-invasive tool that can assess brain function, BOLD signals are often complex to interpret because they result from physiological changes combining both hemodynamic and metabolic effects (Logothetis et al., 2001). Indeed, there is a momentary decrease in blood oxygenation immediately after the neural activity increases, known as the "initial dip" in the hemodynamic response (Hu and Yacoub, 2012). This step is followed by a period where the blood flow increases, not just to a level where oxygen demand is met, but overcompensating for the increased demand. This means that the blood oxygenation actually increases following neural activation. The blood flow peaks after a few seconds and then falls back to baseline, often accompanied by a "post-stimulus undershoot". Another limitation of fMRI is that functional activation studies cannot be performed on freely moving animals. Finally, the cost and size of MR systems can be prohibitive for preclinical research.

Ultrasound imaging has the potential to complement these existing techniques to image brain hemodynamics at a better spatiotemporal resolution and with a reduced cost. Indeed, ultrasound is one of the most widely available technologies used in clinical imaging today. The ultrasound transducer transmits high frequency acoustic pulses into the tissue and record the part of ultrasound energy that is scattered back toward the transducer by various structures in the tissue. The Doppler mode enables ultrasound to detect the motion of blood and to measure the velocity of blood flow based on the frequency shift of the reflected waves from moving red blood cells (RBCs). Even if Doppler ultrasound imaging is intensively used to the study of blood circulation in large vessels in the heart, arteries, limbs, kidney and liver, its use for neuroimaging is still limited. Indeed the skull causes strong attenuation and phase aberration of the beam that reduce significantly the signal-to-noise ratio (SNR) (Clement et al., 2001; Deverson et al., 2000).

Nevertheless, transcranial ultrasound (TCD) is well established in the evaluation of many neurovascular conditions ranging from the diagnostic of cerebrovascular disease and stroke in adults (Sloan et al., 2004) and in pediatrics through the fontanel (Lowe and Bulas, 2005). In adults, a TCD examination requires the use of lower-frequency transducers (typically 2–3 MHz versus 5–10 MHz in infants) to adequately penetrate the calvarium to produce useful gray-scale images and Doppler signals. Even using echo contrast agents (microbubbles) to increase SNR, TCD is limited to a blood flow measurement in large cerebral arteries and veins located close to the natural acoustic windows such as the temporal bone and the foramen magnum (Ries et al., 1991). In pediatrics, high quality images of the brain are acquired through the fontanel because it does not distort or attenuate ultrasound like the skull. However, even in this case, only large blood vessels can be observed with conventional Doppler modes, because the SNR is too low in smaller vessels.

Recently, functional imaging of the whole brain of rodents has been achieved using ultrasound. This emerging tool has been developed along two strategies. The first strategy relies on the injection of microbubbles in the vasculature. These contrast agents generate a stronger and non-linear backscattered signal compared to RBC that can be isolated by a non-linear contrast mode. With this technique, we can monitor CBV changes in the brain microvasculature. Even if this approach allows functional imaging, it requires an invasive surgical procedure including a craniotomy, a tracheotomy and catheterization of the femoral vein and artery that is not compatible with chronic experiments (van Raaij et al., 2011). Moreover, microbubbles have a low intravascular residence times and therefore a constant perfusion is required to maintain a steady concentration.

The second strategy relies on a new sequence for power Doppler imaging that is sensitive enough to detect blood flow in very small vessels without the need for contrast agents (Mace et al., 2011). This new sequence is based on coherent compound imaging (Montaldo et al., 2009), a technique using the emission of ultrasonic plane waves instead of focused beams for acquisition of high quality images at high frame rate. For the attainment of microvascular information, this approach must be combined with an accumulation step. This accumulation step consists of averaging hundreds of time samples acquired during periods smaller than the typical observation time required in brain hemodynamics (typically 1 s). This strategy is suitable for measurement of CBV in the whole brain but required a large craniotomy to observe the brain, which limits its use to acute experiments.

The potential of the technique is huge but it has to be taken a step further to be useful for physiological studies including behavioral tests. The present work describes a thin-skull approach that enables brain ultrasound imaging in chronic conditions. We show that functional activation can be reproducibly and robustly measured during at least 7 days. Then, we characterize the CBV hemodynamic response function (HRF) measured by our new technique and we demonstrate the high sensitivity of the technique by detecting very short – even single impulse – sensory stimuli. With this work, we propose a robust technique for imaging the microvasculature and the brain activity of rodents over time at very high spatiotemporal resolution with a commercially available research ultrasound system.

Materials and methods

Animals

The investigation was performed in accordance with the National Institutes of Health Guide for Care and Use of Laboratory Animals. The protocol was approved by the Local Animal Ethics Committee of Paris Descartes (CEEA 34) registered with the French Ministry of Research and conducted in accordance with Directive 2010/63/EU of the European Parliament. Adult male Sprague–Dawley rats (Janvier Labs, France) weighing 200–300 g were used for this study and were kept in a 12-h dark/light cycle environment at a temperature of 22 °C with ad libitum access to food and water.

Thinned skull surgery

The initial surgery was performed on anesthetized rat by i.p. injection of ketamine (Ketamine 50 mg/mL at 20 mg/kg, Merial) plus xylazine (Rompun 2% at 2 mg/kg, Bayer) diluted in saline (0.9% NaCl). Depth of anesthesia was assessed by pinching the interdigital web of the foot using a forceps. If the animal was responding to a mild stimulation, an extra bolus of 0.5 mL of ketamine (20 mg/kg in saline) was injected. The heart and breathing rates were monitored using a pulse oxymeter (Physiosuite, Kent Scientific). The rhythm and pattern, eye blinking and whisker movements were also used in the overall evaluation of depth of anesthesia. A rectal thermometer was inserted to monitor core body temperature and a heating blanket was placed under the animal during surgery to maintain the body temperature at 37 °C (ATC1000, WPI, USA). The scalp was shaved and cleaned with betadine. The scalp was removed over the entire dorsal skull and then the periosteum was also removed with a scalpel blade. The skin was trimmed laterally and the temporal muscles were gently detached from the bone on both sides of the skull. The frontoparietal bone was thinned on a 1-cm^2 area (from AP $+3.00$ to -7.00 and L $\pm$ 5.00 mm) over the somatosensory cortex at low speed on a dental drill using a 1.4-mm burr (Mesinger). To avoid overheating of the brain, saline was added repeatedly between drilling sessions until the skull becomes flexible and the pial vessels are visible through wet bone. This thickness, which was measured postmortem to be of around 50 μm, is required for ultrasound imaging of the brain in chronic conditions. An echogenic 250-μm glass bead was fixed at bregma 0 with cyanoacrylate glue to provide a landmark to calibrate the position of the ultrasound probe. The complete procedure lasted ~1 h and was immediately followed by μ-Doppler

imaging to assess the quality of the thinned skull procedure. After the imaging session, the bone was protected by a 5 mm thick well of dental cement (Dentalon plus, Heraeus-Kuzler, Germany), cast around the thinned window and filled with low-melting agarose (1%) containing ampicillin at a concentration of 100 μg/mL. The agarose ensured proper acoustic coupling required for ultrasonic imaging and ampicillin was used to prevent bacterial growth after surgery. For recovery following the surgery, the animal was placed in a warm cage and monitored periodically until waked up. For post-surgery analgesia, we provide a buprenorphine injection in i.p. (0.03 μg par g, Buprecare) immediately after the surgery and a second injection 12 h later.

Ultrasound imaging procedure

All images were acquired using a research ultrasound system. This scanner is composed of an electronic module for ultrasound emission and reception (V1, Verasonics, USA), a linear array transducer with a central frequency of 15 MHz (L15-128, 128 elements, 0.1 mm pitch, Vermon, France) and a bi-CPU computer workstation on which custom MATLAB R2012 scripts (MathWorks Inc., USA) are used to generate the pulse wave, to reconstruct all images (including beamforming and filtering steps) and to control the electrical stimulator.

Functional ultrasound imaging was performed at day 0, 2 and 7 days ($n = 4$) after the initial surgery. Rats were anesthetized with isoflurane (1.25% in 100% O_2, 0.5 L/min, Axience) inhaled through a mask covering the mouth and nose. All physiological parameters where monitored during the imaging sessions as described in the previous paragraph.

The stereotaxic frame and the probe were placed on an anti-vibratory table to minimize external sources of tissue vibration. No contrast agents were used. The ultrasound probe was oriented in the coronal plane above the brain and aligned to the region of interest using a piezoelectric linear stage (M403.4DG, Physik Instrumente GmbH & Co. KG, Germany). The acoustic coupling was ensured by isotonic gel (Uni'Gel US, Aspet Inmed, USA) applied between the agarose and the probe.

A single μ-Doppler image of the brain microvasculature in angiogram mode was obtained in 500 ms including 400 ms dedicated to data acquisition and 100 ms for data transfer to the computer. During the first 400 ms, a set of 200 ultrasonic images was acquired at a sampling frequency of 500 Hz (1 image in 2 ms). Each 2 ms image is a compound image reconstructed from 15 tilted plane wave emissions with angles varying from −7° to 7° with a 1° step. The raw data obtained with this sequence was a movie of 200 images $s_R(x, z, t)$ where x is the lateral position, z the depth and t the 200 time points. More details about this ultrasound sequence are presented in Mace et al. (2013).

The signal processing to extract hemodynamics from the movie of 200 images $s_R(x, z, t)$ consisted in a high pass filter of 30 Hz cut-off frequency. This filter removes the slow movements of brain tissue that are generated by respiratory and cardiac pulsations. The filtered signal $s_D(x, z, t)$ is the Doppler signal corresponding to the RBC movements in brain vascular networks. From the Doppler signal we calculated two parameters; the Power-Doppler that is the intensity of the Doppler signal proportional to the CBV in the pixel (μ-Doppler image)

$$I(x,z) = \int s_D^2(x,z,t)dt, \tag{1}$$

and the mean frequency

$$f_m(x,z) = \frac{\int s_D^2(x,z,t)fdf}{\int s_D^2(x,z,f)df}, \tag{2}$$

where $S_D(x, z, f)$ is the frequency spectrum of $s_D(x, z, t)$. The mean frequency provides information about the RBCs' axial velocity v_z that can be computed as

$$v_z = \frac{f_m c}{2f_{us}}, \tag{3}$$

where c is the speed of sound and f_{us} is the ultrasound frequency.

We can also compute the intensity in a subset of Doppler frequencies as

$$I_{(f_{\min},f_{\max})}(x,z) = \int_{f_{\min}}^{f_{\max}} S_D^2(x,z,t)df. \tag{4}$$

Using $f_{\min} = 0$ and $f_{\max} = f_S/2$ we select the intensity of the vessels with a flow going toward the transducer; using $f_{\min} = -f_S/2$ and $f_{\max} = 0$ we select the flow going away the transducer (see Fig. 6B). We can also select ranges of velocities from $v_{\min}$ to $v_{\max}$ using $f_{\min} = 2v_{\min}f_{us}/c$ and $f_{\max} = 2v_{\max}f_{us}/c$.

For functional imaging, μ-Doppler images were acquired at 2 Hz during the stimulation paradigm. The only difference with the 'angiograms' described above is that we used 5 tilted plane waves (angle from −7° to 7° with 2° steps) repeated 3 times instead of 15 different angles per ultrasonic image (see Fig. 3A). This allowed us to reduce the time needed to process images (beamforming step) with a little effect on image quality. The dead time between acquisitions (100 ms) is dedicated to the processing of all ultrasonic images online and to their storage on the memory disk for off-line analysis. With our custom system, this dead time was significantly shortened compared to a previous work (3 s minimum) (Mace et al., 2013), which led to an improved temporal resolution (increased by a factor 6) to follow CBV changes. For each trial, the output of functional imaging is an image sequence $I(x, z)$ proportional to CBV.

Electrical stimulation

Electrical stimulus pulses (200 μs pulse width, 1 mA intensity, 5 Hz repetition frequency) were generated using a microcontroller (Uno, Arduino, Italia) controlled by MATLAB and delivered using a constant current isolator (DS3, Digitimer Ltd., U.K.) to one forepaw using 2 needle-electrodes (Biopac Systems, Inc., USA) inserted under the palmar skin between digits two and four. For functional imaging, each trial consisted of a 35 s pre-stimulus baseline period followed by a stimulus of 25 (5 s), 10 (2 s), 5 (1 s) or 1 pulse(s) and a post-stimulus period for a total duration of 50 s. The minimum time interval between two trials was 1 min. Five to ten trials were repeated for each type of stimulus during an imaging session.

Analysis of hemodynamics

Off-line analyses of functional images were performed using dedicated MATLAB scripts. For each trial, the pixel signal was first normalized with the pixel prestimulus average (I_{init}). A pixel was considered as activated if the signal crossed a threshold value defined as $I_{init} + 1.5\sigma$ where σ is the standard deviation during the prestimulus period. The map of activated pixels was smoothed to eliminate outliers with a gaussian spatial filter of 5×5 pixels. To calculate the HRF, the signal was averaged in the operator-independent region of interest defined by all activated pixels. Time to peak (TTP), full width at half-maximum (FWHM), peak amplitude (PA) and onset time (OT) were calculated after a 16-fold Fourier interpolation of the HRF. Spatial activation maps display all activated voxels superimposed on a reference μ-Doppler image.

For the study of anticorrelated signals, correlation maps were built showing the correlation coefficient between the Doppler intensity

signal and the stimulus pattern for each pixel. Temporal profiles were then averaged in two regions of interest defined as the contralateral and ipsilateral forepaw S1 regions extracted from the Paxinos atlas (Paxinos et al., 1985).

Extracellular recordings

On one animal, we measured the extracellular response evoked in forelimb somatosensory cortex (S1FL) for each stimulation paradigm. A 1 mm^2 cranial window was performed on the thinned skull over the S1FL. A quartz-insulated platinum-tungsten electrode (2 to 5 MΩ) was inserted into the cortical tissue (750 μm deep) using a Eckhorn mini-matrix microdrive system (Thomas Recordings). The electrode is thin (60 μm shaft; 10 μm tip diameter), but strong enough to penetrate the dura, thus reducing the damage to the neural tissue. Evoked FP (eFP) signals were acquired at a 1 KHz sampling rate without filtering, amplified, digitized with the aid of CED hardware and Spike 2 software (version 7, Cambridge Electronic Design). Electrical forelimb stimulation did introduce a short, high frequency deflection into the data, such that the data surrounding stimulation onset between −1 and 2 ms were discarded. Ten trials were acquired for each condition (1, 5, 10, or 25 pulses). For each trial, the eFP amplitude and the ΣFP response (Masamoto et al., 2007) were measured.

Immunohistochemistry

After the last imaging session, rats were deeply anesthetized with sodium pentobarbital (100 mg/kg i.p.) and transcardially perfused with 50 mL saline followed by 150 mL of 4% paraformaldehyde in 0.1 M phosphate buffer saline (PBS), pH 7.4, using a peristaltic pump and flow rate of 10 to 25 mL/min. Brain was removed and placed overnight in the 4% paraformaldehyde fixative in PBS, then 40 μm thick sections were prepared using a vibratome (Leica VT1000S, Leica Microsystems, Germany). Slices were immunolabeled overnight with antibodies against the neuronal marker NeuN (1:1000; Millipore, USA), the astroglial marker GFAP (1:500; Invitrogen, USA), and the microglial cell marker Iba1 (1:500; Wako, Japan). Then slices were washed 3 × 10 min at room temperature followed by incubation with species-appropriate secondary antibodies conjugated to Alexa Fluor 488 nm or 594 nm (Molecular Probes, Life Technologies, France, 1:1,000) in PBS, washed again (3 × 10 min) in PBS, and mounted with a DAPI Prolong Antifade kit (Molecular Probes, Life Technologies, France). Standardized image acquisition was performed with an Axio Imager Z1 (Zeiss, France).

Statistical analysis

The intensity of the power Doppler was represented as the percentage of change relative to the baseline in the activated region ± standard deviation (SD) or ± standard error of the mean (SEM) for the analysis of spatial evolution of the activated area. Statistical analyses were performed using a Prism 6 (GraphPad software) Student's *t* test. The levels of significance were set at: (*) $p < 0.05$, (**) $p < 0.01$, (***), $p < 0.001$ and (****) $p < 0.0001$.

Results

Chronic ultrasound imaging through a thinned skull window

We first tested the feasibility of imaging the rat brain microvasculature with our ultrasound system in chronic conditions.

A schematic view of the setup is shown in Figs. 1A and B. The ultrasonic probe is oriented in the coronal plane above the thinned skull. For comparison, Fig. 1 presents the ultrasonic images obtained in 3 different experimental conditions: with an intact skull (Fig. 1C), after a craniotomy (Fig. 1D) or after thinned skull surgery (Fig. 1E). Standard ultrasonic images, obtained with the B-Mode, give a measurement of tissue echogenicity whereas angiograms, obtained with the μ-Doppler mode, quantify the CBV in each pixel. This last mode was specifically developed for high-resolution and high signal-to-noise ratio (SNR) imaging of the brain microvasculature. Each μ-Doppler image has an in-plane spatial resolution of 100 μm, a slice thickness down to 500 μm and is acquired in 400 ms.

In a control rat, the intact skull strongly attenuates the high frequency ultrasonic waves (15 MHz) sent by the probe. The skull appears hyper-intense on the B-Mode and no contrast is observed into the brain. Similarly, no cerebral vessels are detected on the μ-Doppler image.

After removal of the skull bone, the μ-Doppler mode allows for the observation of the rat brain microvasculature in its entire depth including the cortical blood vessels perpendicular to the brain surface, a less well-perfused region corresponding to the white matter (corpus callosum; cc) and subcortical regions (striatum; Cpu) with vessels oriented in various directions. This invasive technique has already been tested and produced similar images than with our imaging system (Mace et al., 2011). It is noticeable that, even when the skull is removed, B-Mode images exhibit very little contrast between different brain structures, except for the ventricles that are echogenic as observed in Fig. 1D, which limits its interest in neuroimaging.

To overcome side effects occurring after a craniotomy such as severe damage to parenchyma and inflammation (Cole et al., 2011), we developed a dedicated surgical procedure for chronic ultrasound imaging in physiological conditions. Briefly, we thinned the skull on a 1 cm^2 large area with a low-speed burr (AP = ß + 4 mm to −6 mm, L = midline ± 5 mm) to a final thickness of around 50 μm to reduce signal attenuation associated with bone structure. The bottom right panel in Fig. 1E presents ultrasound images obtained just after the thinned skull surgery (day 0). In B-mode the skull surface is offsetting the shape of the brain and appears less bright confirming a significant reduction in the signal scattering. Moreover, μ-Doppler images remained of equivalent quality compared with craniotomy but with a soft background noise. For one animal, we extracted the skull postmortem and measured experimentally the attenuation induced by the thinned bone. The attenuation levels ranged from 8 to 20 dB, with an average value of 12 dB (data not shown). The attenuation may vary between rats according to the surgical finesse and the position of the ultrasonic probe during the experiment but was sufficiently low to provide high quality angiograms and functional images.

A critical physiological assessment of the thin skull window concerns the potential brain inflammation and neuronal cell death caused by compression of the meningeal space during surgery (Roth et al., 2014). We controlled the expression of Iba1 and glial fibrillary acidic protein (GFAP), which are upregulated in reactive macrophages/microglia and astrocytes, respectively, during brain injury (Drew et al., 2010). As shown in Fig. 2, the pattern of immunostaining for both antibodies was weak and the morphology and density of these cells were similar to the control between day 2 (not shown) and day 15 after surgery, which corresponds to the period of high inflammation caused by craniotomy (Xu et al., 2007). Moreover, NeuN antibodies do not show a difference in neuronal density in the cortex between the thinned skull (609 ± 54 neurons/mm^3, 3 animals) and the control rat (622 ± 68 neurons/mm^3, 3 animals) confirming the absence of neuronal death. The microglia, astrocytes, neuron labeling and vascular data all together showed that the thinned skull procedure did not induce an inflammatory response or neuronal cell death. We demonstrate that μ-Doppler imaging should be performed in chronic conditions while preserving the good spatial resolution in the imaging plane (up to 100 μm) and the sensitivity.

To demonstrate that our protocol allows for ultrasound brain imaging in chronic conditions, we performed μ-Doppler and functional imaging during 3 independent imaging sessions at days 0, 2, and 7 after surgery on the same animals (n = 4). We did not observe any difference

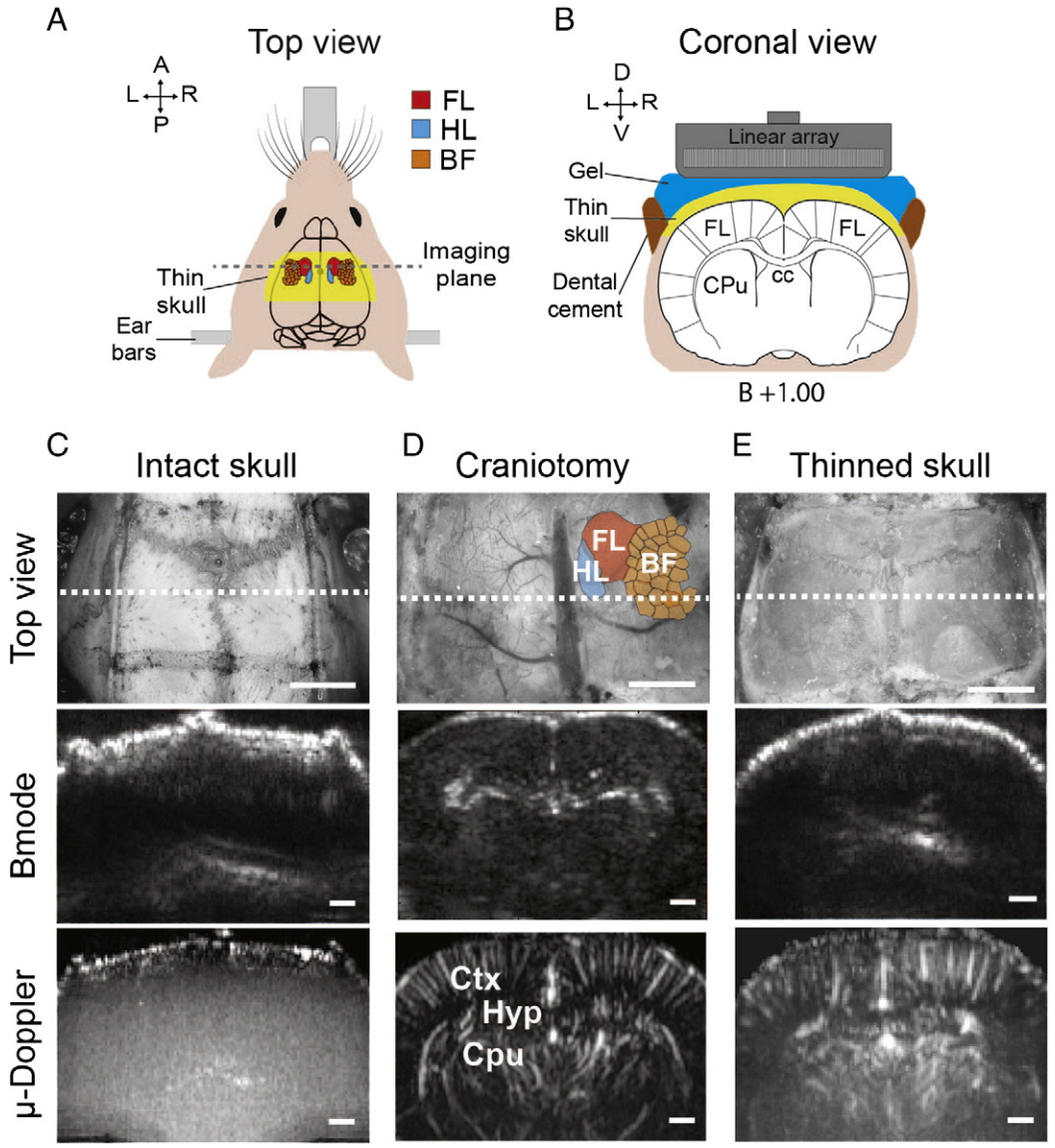

Fig. 1. Experimental setup. (A) Schematic top view of the setup. The dotted line indicates the position of the probe during functional ultrasound imaging (Bregma + 1.00). The yellow area represents the region of the thinned skull. The position of the primary somatosensory forelimb (FL), hindlimb (HL) and barrelfield (BF) cortex is highlighted according to the brain atlas. (B) Coronal view of the setup. Atlas image showing the cross section of the rat brain imaged by the ultrasound probe. (C) (D) and (E) A typical result of ultrasound imaging performed in 3 different experimental conditions: intact skull, after a large craniotomy and after the thinned skull surgery, respectively. The upper panel represents a top view picture of the skull. The white dotted line indicates the position of the probe during functional ultrasound imaging (Bregma −3.00). The central panels show the B-mode images and the bottom panels show the μ-Doppler images. Ctx: cortex, Cpu: striatum; Hyp: hippocampus. Scale bar is 0.5 mm.

on μ-Doppler images or functional images during these 3 sessions. The image quality and the brain vasculature topology were identical. Therefore, in the following paragraph, we pooled the results obtained at different time points. With these results, we demonstrate that the thinned-skull procedure is a minimally invasive surgery that allowed for stable and high quality brain ultrasound imaging for at least 7 days.

Functional ultrasound imaging

Functional brain imaging relies on the localization of brain activity based on an increased blood volume due to neurovascular coupling (Roy and Sherrington, 1890). Functional ultrasound imaging uses the power of the Doppler signal that is proportional to the number of RBCs producing the Doppler echoes (Shung et al., 1976) and therefore to the CBV (see Materials and methods). As presented in Fig. 3A (bottom panel), for each trial we record 60 μ-Doppler images that give a 30 s movie of the CBV response evoked by a non-noxious electrical stimulation of the forepaw (Fig. 3A top panel).

First we present the results obtained with the longest stimulus duration (25 pulses, 5 s). These parameters were chosen for best response by rat forepaw stimulation under isoflurane anesthesia according to literature (Kim et al., 2010).

Fig. 3B shows a single μ-Doppler frame from a functional movie. Images were recorded 1 mm anterior from bregma, a coronal plane that comprises the forelimb sensorimotor cortex according to rat stereotaxic atlas (Paxinos et al., 1985). Signal in blood vessel is clearly detected in both cortical and subcortical areas.

Fig. 3C shows the averaged temporal profile of the CBV HRF pooling the results from the 4 animals, recorded at days 2 and 7 after the surgery with 5 trials per imaging session, so a total of 40 functional movies. In the supplementary material, a movie of a typical functional ultrasound imaging dataset is shown. We emphasized that this movie corresponds to only one forepaw stimulation (5 s duration) without averaging. The hemodynamic response associated with a single trial stimulus is easily detected by this technique. We excluded from the analysis the results at day 0 because the experiments were performed under ketamine/

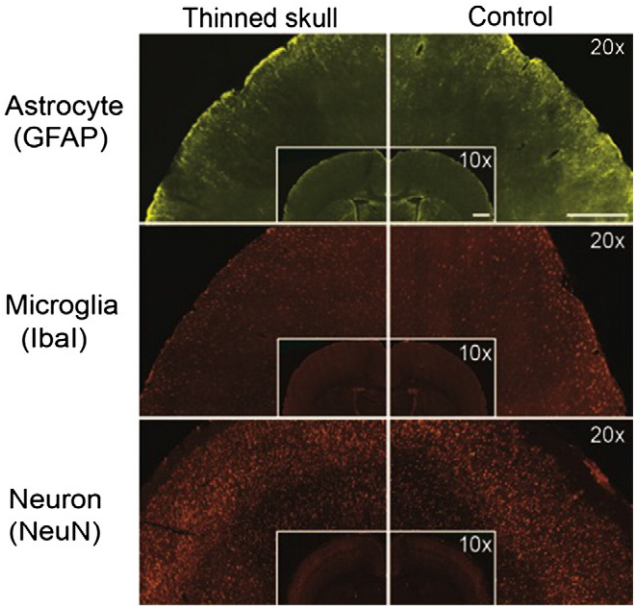

Fig. 2. Evaluation of brain inflammation after the thinned skull surgery. Fluorescence microscopy images of astrocytes (GFAP); microglia (Iba1) and neurons (NeuN) from the somatosensory cortex of the rat 10 days after the surgery (left panels) compared with the control rat (right panels). Both widefield (10×) and higher magnification images (20×) show similar basal levels of expression of NeuN, GFAP and Iba1 markers in the cortex (n = 3). We did not observe any change in the morphology of GFAP positive cells. Scale bar, 0.5 mm.

xylazine anesthesia instead of isoflurane and it has been extensively reported that anesthesia has broad effects on spatial propagation, temporal dynamics and quantitative relationship between the neural and vascular responses to cortical stimulation (Masamoto and Kanno, 2012).

We first analyzed the evolution of the CBV in 2 symmetrical regions of interest (ROI) based on the rat brain atlas corresponding to the forelimb somatosensory cortex (S1FL) in the contralateral and ipsilateral hemispheres respectively (Fig. 3B). The curves are presented in Fig. 3C. As expected from physiology, we observed a large increase of the CBV HRF in the contralateral hemisphere in response to 25 electrical pulses (5 s long stimulus) in the right forepaw. CBV curves consistently show a monophasic shape with a prolonged and slowly decaying tail that remains elevated for several seconds beyond the duration of the task (for clarity, only the first 15 s post-stimulus were shown). We did not observe significant differences in the temporal characteristics of the CBV HRF between day 2 and day 7 confirming the absence of effects on brain hemodynamics of the thinned-skull surgery. The CBV response reached its maximal change of 13.3 ± 5.8% at 5 s after stimulus onset (Fig. 3C, red curve). We also confirmed that no ipsilateral activation of the forelimb cortex was detected with the right forelimb stimulation (Fig. 3C black curve). These results are in good agreement with studies performed using various functional imaging modalities such as BOLD or CBV fMRI (Silva et al., 2007), optical intrinsic imaging (Berwick et al., 2008) or laser Doppler flowmetry (Malonek et al., 1997).

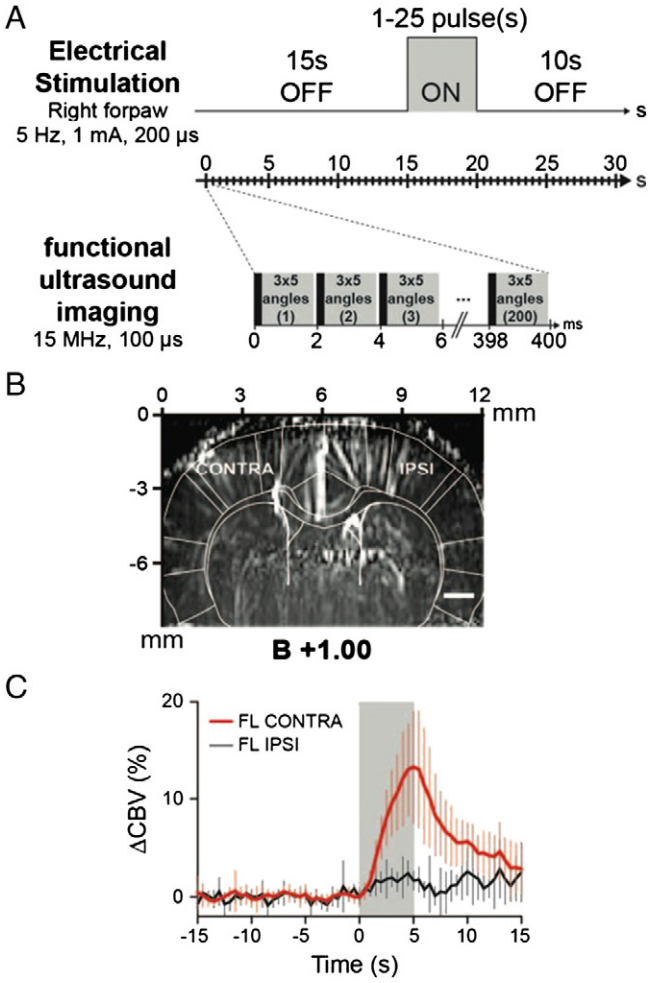

Fig. 3. Measurement of the CBV HRF after somatosensory evoked stimulation of the forepaw. (A) The stimulation paradigm was composed of a 15 s pre-stimulus baseline followed by a stimulation period (gray shaded bar) and a 10 s post-stimulus period. We tested 4 stimulation durations: 5 s (25 pulses) or 2 s (10 pulses) or 1 s (5 pulses) or 200 µs (1 pulse) with the same intensity (1 mA), pulse width (200 µs) and repetition frequency (5 Hz). Functional imaging ultrasound was performed during the paradigm: 60 µ-Doppler images are recorded, each composed from 200 ultrasonic images acquired at 500 Hz frame rate. (B) Example of one power Doppler image. Anatomical brain outlines showing ipsi and contralateral FL are superimposed. Scale bar, 500 µm. (C) Average CBV HRF (40 trials) measured in the two anatomical ROIs for a 25 pulse stimulation. Error bars indicate 1 SD.

Temporal characteristics of the CBV HRF to short stimulations

Functional ultrasound imaging performed with this ultrasound system has a temporal resolution of 2 frames per second, which enables the temporal characterization of the CBV HRF after interpolation. Based on the above observation that a significant increase of the CBV can be detected for a 5 s stimulus duration, we set out to determine the sensitivity of our imaging technique by reducing the length of the stimulus. We performed these tests on the same group of animals: the stimulus was randomly varied among 1, 5, 10 or 25 electrical pulses and repeated at least 5 times for a total run time of 60 min. As in the previous paragraph, the CBV HRF and eFP time traces shown in Fig. 4B correspond to single-response time series that were first averaged between each subject and then across all subjects to increase the statistical power of the analytical procedures (40 trials in total per condition).

Fig. 4B is an overlay of the CBV HRF for each condition. In this figure the ROI was defined by the significantly activated pixels for each trial (see Materials and methods). It avoids the use of anatomical ROI that are often too large compared to truly active voxels. Fig. 4A shows an example of the ROI outline for a 25 pulse stimulus. In these conditions, we measure a 19.3 ± 7.1% increase of the peak amplitude of the CBV HRF in response to a 25 pulse stimulus. As observed using CBV fMRI (Hirano et al., 2011), a reduction of the stimulus to 10 and then to 5 electrical pulses leads to a subsequent decrease of the peak amplitude to 11.3 ± 4.3% and 7.8 ± 1.9% respectively.

Reducing the duration of the stimulus is very important to assess the sensitivity of the technique, but also to get as close as possible to a more physiological sensory stimulation. Indeed, in this specific case, electrical forepaw stimulation results not only in sensory but also in proprioceptive input owing to mild muscle and joint movements, whereas tactile

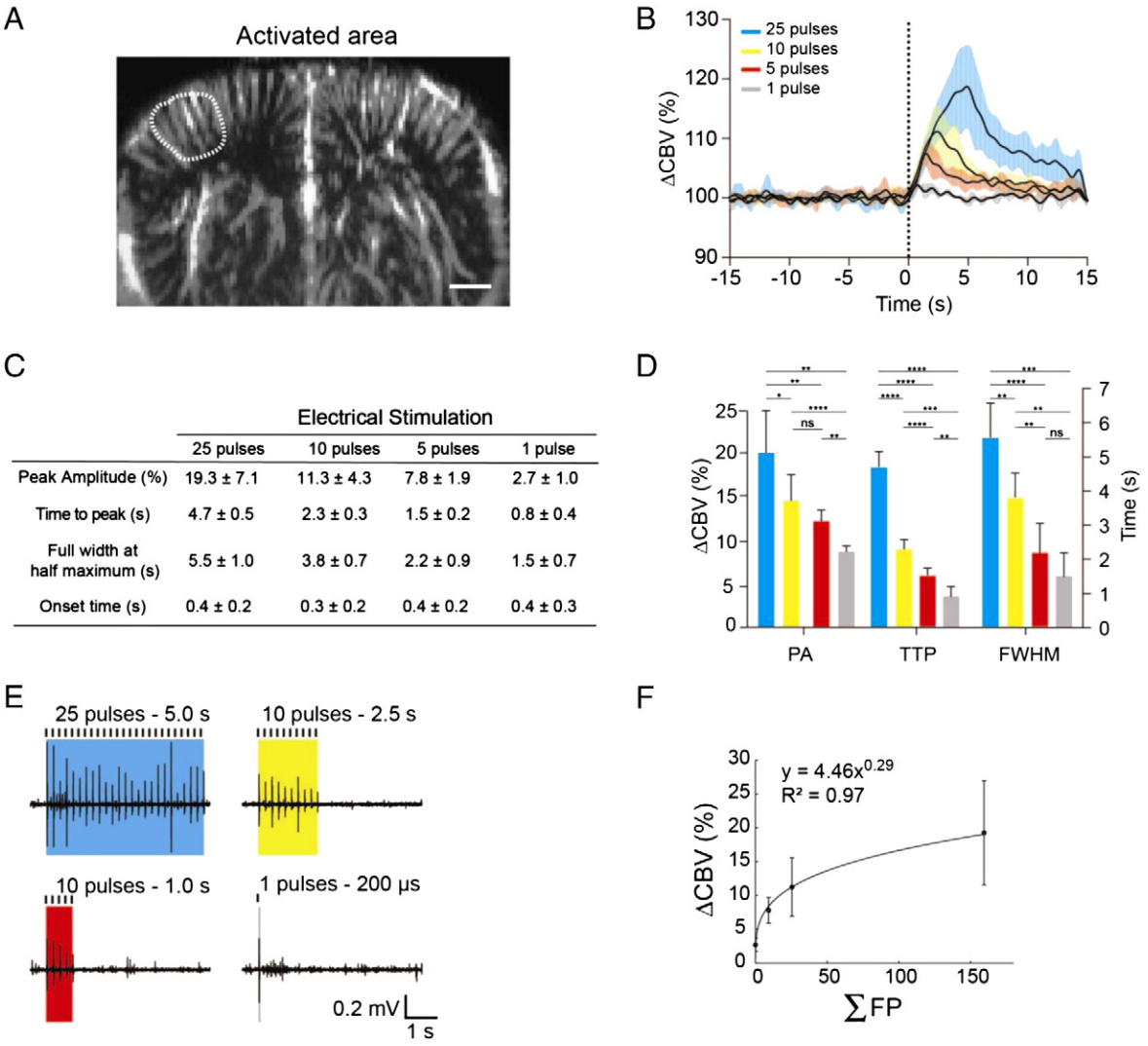

Fig. 4. Temporal characteristics of the CBV HRF. (A) Representative activation map showing the outline of the activated region (dashed line) at the peak of the CBV response for a 25 pulse stimulus. (B) For each stimulus paradigm, average CBV HRF calculated within the corresponding activated area (40 trials for each curve). Error bars indicate 1 SD. All stimuli elicited a response. (C). Parameters of the CBV HRF from curves in (B). Mean peak amplitude (PA), time-to-peak (TTP), full width at half maximum (FWHM) and onset time (OT) calculated for each stimulus. (D) Graph of the HRF parameters including the statistical analysis. PA, TTP and FWHM monotonically decrease when the stimulus duration decreases. Error bars indicate 1 SD. $^{****}p < 0.0001$, $^{***}p < 0.001$, $^{**}p < 0.01$, $^{*}p < 0.05$, ns: non-significant, Student's *t*-test. Note that a single impulse was sufficient to induce a detectable CBV change. (E) Representative eFP traces for 25 pulses (blue shaded bar), 10 pulses (yellow shaded bar), 5 pulses (red shaded bar) or 1 pulse (gray shaded bar) stimulus. (F) CBV increase as a function of neuronal activity (measured by ΣFP), fitted by a power law.

stimulation does not. It has been demonstrated that this effect might be reduced when decreasing the number of pulses (Van Camp et al., 2006). Therefore, we tried a single 200 µs electrical impulse stimulation. As shown in Fig. 4B, functional ultrasound imaging is sensitive enough to detect a 2.7 ± 1.0% increase of the CBV associated with such an ultrashort stimulus.

Longer stimulus durations such as 50 or 75 pulses produced no additional increase in the peak amplitude of the CBV HRF compared to 25 pulses (data not shown). The CBV HRF displayed a prolonged and slowly decaying offset tail, which is visible for stimulus duration as short as 5 pulses. These results are in agreement with similar experiments performed using CBV fMRI (Silva et al., 2007). We did not find neither initial dip nor post-stimulus undershoot in response to all stimulus durations as sometimes observed in optical or BOLD fMRI studies (Hu et al., 1997). This is coherent with the fact that we measure CBV, a hemodynamic parameter that is insensitive to blood oxygenation contrary to BOLD signals.

Fig. 4C presents in details the temporal characteristics of the CBV HRF including the onset time (OT), time-to-peak (TTP), full width at half-maximum (FWHM) and peak amplitude (PA) reported as mean values and standard deviations across subjects for each stimulation paradigm. As confirmed by the statistical analysis of these results presented in Fig. 4D, it should be noted that TTP, FWHM and PA of the evoked CBV HRF are dependent of the length of the stimulus: all these parameters were significantly increased with an increase of the number of stimulus (i.e. TTP = 4.7 ± 0.5 s for pulses vs. 2.3 ± 0.3 s for 10 pulses, 1.5 ± 0.2 s for 5 pulses and 0.8 ± 0.4 s for 1 pulse). On the contrary, the OT of the CBV HRF remains constant with an average value of 0.4 ± 0.2 s that is independent of the stimulus length.

Electrophysiological information is required to go further in the physiological interpretation of the hemodynamic changes previously observed. On one animal, we recorded local field potentials evoked in S1FL for each stimulation paradigm. Fig. 4E shows example traces of eFP response for the various stimulation conditions. In general, the first evoked FP was the largest among all consecutive FPs for 25, 10 and 5 stimulations. The following eFP responses were either constant or attenuated with a gradual adaptation, such that the amplitude at the end of stimulation was never below 40% that of the initial response.

The evoked FP consisted of an EPSP followed by a prolonged biphasic IPSP. We observed a peak amplitude of ~0.45–0.50 mV that occurred ~15–20 ms after an electrical stimulation. The amplitude was measured between the first positive peak and the negative peak of the trace (data not shown).

Then, we calculated the ΣFP, that is, the product of eFP amplitude, stimulus rate and stimulus duration to better quantify the total FP response. This parameter is proportional to the number of pulses, as expected from the literature (data not shown). Fig. 4F represents a plot of the ΣFP in function of the CBV increase and shows that the evolution is non-linear. We fitted this curve by a power law with a R^2 coefficient of 0.97.

As previously described by many groups, we observed a strong temporal shift between neural and μ-Doppler hemodynamic responses acting like a low pass filter, smearing out changes in the local electrical activity. For the single impulse stimulus, the eFP peaks around 15 ms whereas the HRF peaks around 400 ms.

Spatial evolution of CBV HRF evoked by forepaw stimulation

Fig. 5A shows the maximal extent of the activated area after the right forepaw stimulation of various durations averaged on all trials. Here again, we observed a correlation between the length of the stimulus and the size of the activated area. Indeed, a 25 pulse-long stimulus (blue area) gives rise to an activated area with a maximum size of 4.1 ± 0.9 mm^2 that spreads beyond the boundaries of the S1FL cortex. Comparatively, a 10 pulse stimulus (yellow area) leads to a 41% decrease of the size of the previous activated area (2.5 ± 0.6 mm^2) still spreading in the entire thickness of the cortex. In contrast, a 5 pulse short stimulus (red area) leads to a clear diminution of the size of the activated area (1.0 ± 0.6 mm^2) with a peak response distributed only in layers II–III and IV of the cortex. Area for single pulse stimulation is not shown because we observed a high variability between trials.

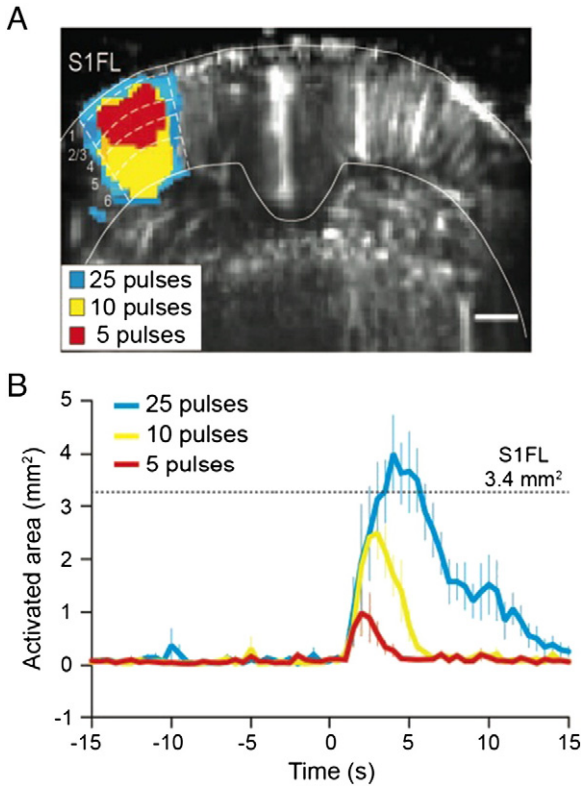

Fig. 5. Spatial characteristics of the CBV HRF. (A) Average maximal activated area (10 trials) for 25 pulses (blue area), 10 pulses (yellow area) or 5 pulses (red area) in one animal. This image is overlaid on a μ-Doppler image and the dashed lines outline the anatomical layers of the cortex. Scale bar, 0.5 mm. (B) Evolution of the size of the activated area in response to 25, 10 or 5 pulse stimuli. The dashed line represents the size of the FL cortex measured at Bregma +1.00 according to the rat brain atlas. Error bars indicate 1 SEM.

Fig. 5B shows the area of activated pixels as a function of time for each experimental condition. For all paradigms that were tested, we observed a biphasic profile – a fast onset time and a longer offset delay – that is strongly correlated to the CBV HRF time curves described in Fig. 4B. Indeed, the size of the activated area reaches a maximal value at 4.1 ± 0.4 s (25 pulses), 2.0 ± 0.3 s (10 pulses) and 1.3 ± 0.2 s (5 pulses) after stimulus onset. This values match with those observed for the CBV HRF (Fig. 4C).

Quantitative hemodynamic parameters in the cortical arterioles and venules

All data presented previously are extracted from the power Doppler signal that quantifies the total blood volume. But μ-Doppler is also suitable to assess the amount of blood flowing up or down based on a quantitative spectral separation of the Doppler signal.

A typical Doppler spectrum of the cortical vasculature (averaged on a small 10 × 10 pixel ROI) is presented in Fig. 6A. The signal is composed of a positive (right) and a negative (left) signal that are proportional to the number of RBCs flowing toward and away from the transducer, respectively. As observed in Fig. 6A, very low frequencies were eliminated by a high pass filter (gray bar) with a 30 Hz cutoff frequency that was used to remove the noise coming from tissue motion and animal breathing. A consequence is that neither capillary blood nor blood vessels containing RBCs with an axial velocity lower than 1.5 mm/s are detected by μ-Doppler imaging.

Fig. 6B presents a typical color-coded μ-Doppler image from a coronal slice of the rat brain in resting state. The amount of CBV flowing up is assigned to the blue color while the amount of CBV flowing down is assigned to the red color for each pixel. The CBV magnitude (normalized by the maximal value in the image) is represented by gradients of brightness of the assigned color and both color bars are presented on the right of the image. In the cortex, arterioles and venules are oriented perpendicularly to the pial surface and therefore lie in the axial direction of the ultrasound beam. They are very well discriminated with this representation.

We measured a comparable number of penetrating veins and arterioles using μ-Doppler (data not shown). This result is not in agreement with the average factor 2 venules per arteriole previously reported in rodents (Nguyen et al., 2011; van Raaij et al., 2011; Woolsey et al., 1996) but may be explained by the low velocity of RBC observed in ascending venules (Shih et al., 2012) that are therefore below the detection threshold given by the filter.

On top of the CBV, the mean velocity of RBCs in each pixel can also be measured with μ-Doppler. It is directly linked to the central frequency of the Doppler spectrum (see Materials and methods). Fig. 6C presents the changes in mean RBC velocity in the activated cortical area after evoked stimulation of the forepaw using 25, 10 or 5 pulses. We observed that both venous and arterial flows show a mean RBC velocity increase of similar amplitude compared to the prestimulus period, for the three conditions tested. Moreover, we measured a significant difference between 25 and 5 pulses with a velocity increase that goes from 1.2 ± 0.3 mm/s to 0.5 ± 0.1 mm/s for arteries and from 0.7 ± 0.2 mm/s to 0.45 ± 0.05 mm/s for venules. These results demonstrate that there is a significant change of the RBC velocity, which depends on the duration of the stimulus. This is in agreement with results obtained with CBF fMRI (Hirano et al., 2011).

To examine whether RBC velocity is fairly distributed in cortical vessels during functional activation, we analyzed in more details hemodynamic responses for a 25 pulse long stimulus. This paradigm was chosen because it elicits robust hemodynamic responses with a maximal increase of the CBV. We split the functional movies in two ranges of RBC velocity including a “slow” range from 1.5 mm/s to 7.0 mm/s and a

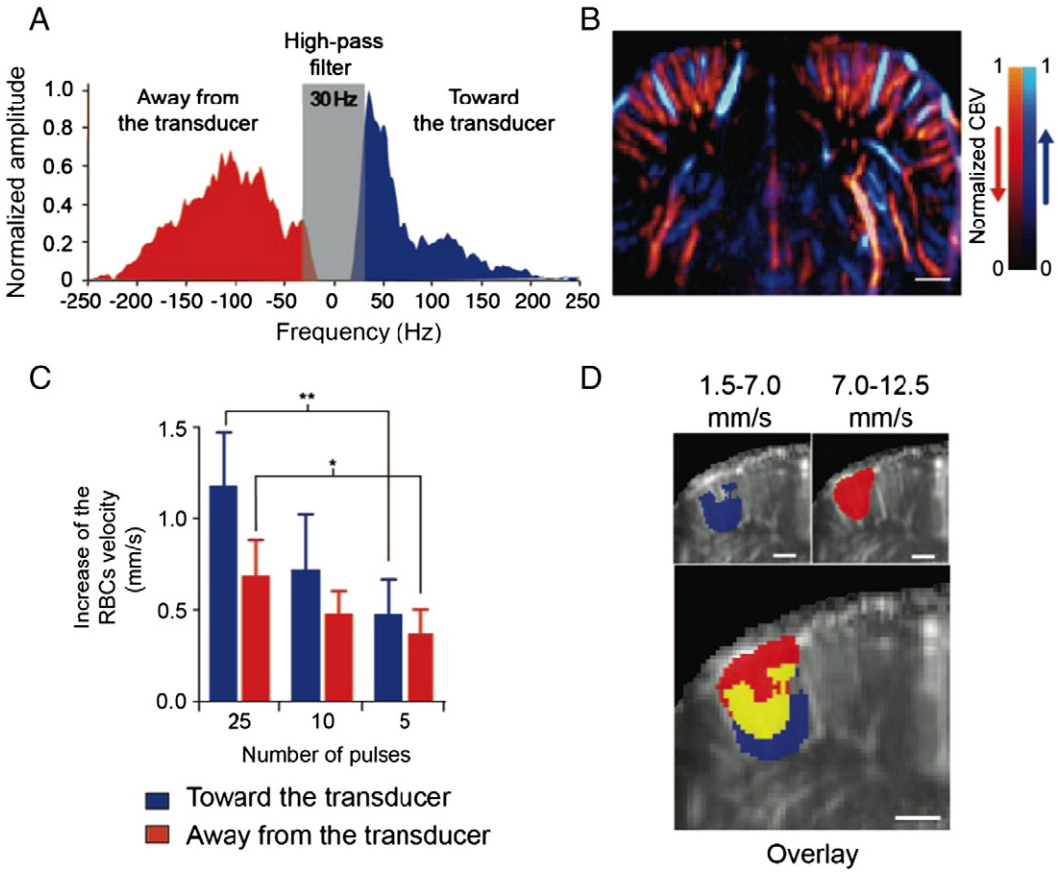

Fig. 6. Analysis of RBC velocities in the cortex during the functional activation of the brain. (A) Typical Doppler spectrum obtained from an ROI of 10 × 10 pixels in the cortex. The positive (blue) and negative (red) frequencies are due to RBCs flowing toward or away the transducer, respectively. In the cortex, penetrating arterioles produce negative frequencies (red) and ascending venules positive frequencies (blue). (B) Color coded μ-Doppler image representing in blue the amount of CBV flowing up and in red the amount of CBV flowing down in each pixel. Scale bar, 0.5 mm. (C) Maximal increase of RBC velocity during different stimulations (mean ± SD, $^{*}p < 0.05$, $^{**}p < 0.01$, Student's *t*-test). (D) Map showing the activated area obtained when using only the 1.5 to 7.0 mm/s RBC velocity range (in blue) or the 7.0 to 12.5 mm/s range (in red) for a 5 s long (25 pulses) stimulus (one animal, 10 trials). Yellow area located in the middle of the cortex shows the overlapping of the two regions. Scale bars, 0.5 mm.

"fast" range from 7.0 mm/s to 12.5 mm/s using the Eq. (4) (see Materials and methods). Then, we recalculated the activated area corresponding to each range.

As observed in Fig. 6D bottom panel, the activated area is spatially segregated in 2 sub-regions depending on the velocity range. The slowest component (1.5 to 7.0 mm/s in blue) is mainly located in deeper cortical structures, while the fastest component (7.0 to 12.5 mm/s in red) is observed in upper layers I, II and III. In the middle of the cortex both velocity ranges contribute to the CBV HRF. These maps were averaged on all animals and all trials. These results were consistently observed in chronic condition over a period of 7 days in the same animals.

Discussion

The main finding of this paper is that ultrasound imaging is an efficient tool to perform angiography and/or functional rat brain imaging at high spatiotemporal resolution in chronic conditions. Having developed a dedicated thinned skull surgery, we demonstrated that microvascular hemodynamics could be imaged in the cortex and in subcortical regions at least 7 days on the same animal. We then investigated the temporal and spatial properties of the CBV HRF evoked by a mild electrical stimulation of the forepaw ranging from 5 s (25 pulses) to 200 μs (single impulse). The sensitivity of the technique is sufficient to image the response evoked in a single trial, as illustrated by the movie in the supplementary data. We then pooled all results to observe the statistical trends of the HRF. Temporally, we observed a more intense and prolonged HRF when the stimulus duration increases. Spatially, we observed an enhancement of the activated cortical area with stimulus duration. Interestingly, we could detect the activity evoked by a single electrical impulsion in the forepaw, which elicited a peak response 400 ms after stimulus onset. When compared to the electrophysiological response (FP), we see that the HRF is much slower and does not increase linearly with neuronal evoked response, which is expected from results obtained with other imaging methods.

With the same data, it is also possible to measure blood velocities. In the cortex, blood velocity increased both in arterioles and venules during activation. Longer stimulus duration give rise to a bigger increase of the RBCs' velocity. When looking the spatial distribution of mean RBCs' velocities, we observed that the fast RBCs' velocities (>7 mm/s) are located in superficial layers of the cortex whereas the slow velocities (<7 mm/s) are located in deeper cortical layer. This could mean that bigger vessels contribute to the HRF mainly in the upper part of the cortex whereas smaller vessels are the main contributors to the HRF in the deeper layers.

Advantages and limitations of chronic functional ultrasound imaging

Compared to other modalities for blood flow imaging in living rodent, functional ultrasound imaging has a spatial resolution of 100 μm in the plane with a 500 μm thickness that is better than both fMRI and PET. A main advantage compared to other ultrasound modalities such as functional micro-ultrasound (fMUS) is that it does not require the use of microbubbles contrast agents and therefore is more suitable for chronic experiments. After the initial surgery, no preparation of the

animal is needed before an imaging session. On the contrary to optical methods such as intrinsic optical imaging (IOI), voltage sensitive dye imaging (VSDi) or 2 photon microscopy (2 PM), chronic functional ultrasound imaging is not limited to the cortical surface but provides CBV measurement in the whole depth of the brain. Concerning the temporal resolution, in the version of our imaging system used here, the maximal imaging frame rate that we could achieved was 2 Hz because of the high computational power required to process μ-Doppler images. This processing time is rapidly decreasing thanks to parallel computing (Yiu et al., 2011). We are confident that functional ultrasound imaging could soon be performed in real-time and with enough storage capacity to record hemodynamic brain activity during several hours. Such increased of the computing performance also opens perspective for 3D imaging by using 3 dimensional matrix of transducers.

One of the strongest assets of functional ultrasound is that it holds potential in the near future for brain imaging of freely moving conditions. The ultrasonic probe can be miniaturized and implanted on the head of rodents. The chronic recordings presented in this paper are an important first step toward this end.

Hemodynamic parameters during functional activation of the cortex

The spatiotemporal characteristics of the hemodynamic response in the cortex have been extensively studied using an electrophysiological measurement in combination with a large variety of imaging techniques such as IOI (Devor et al., 2003; Sheth et al., 2003), CBV or BOLD fMRI (Hoffmeyer et al., 2007; Logothetis et al., 2001; Silva et al., 2007) or laser Doppler flowmetry (Hoffmeyer et al., 2007). These studies led to different conclusions with respect to the coupling between neuronal activity and the hemodynamic response. These discrepancies are partially due to methodological differences but indicate that a more precise imaging method is required to better understand the neurovascular coupling. Functional ultrasound is a good candidate because this imaging modality can assess CBV changes in the entire depth of the cortex and in subcortical areas with a high spatiotemporal resolution and a high sensitivity.

The μ-Doppler signal can be considered as a pure hemodynamic signal that is proportional to the number of RBCs in the voxel and should be further compared with the vascular-space-occupancy (VASO) MRI method that predominantly reflects total parenchymal CBV without requiring injection of contrast agents (Lu and van Zijl, 2012; Lu et al., 2003). Such as VASO MRI, micro-Doppler imaging is particularly useful in situations in which a pure contrast mechanism is desirable, as the more widely used BOLD signal reflects a combination of multiple variables, including CBV, CBF, $CMRO_2$ and baseline venous oxygenation. CBV can also be measured by MRI and used to probe functional activation. However, the most common method requires the injection of contrast agents. Other techniques such as vascular space occupancy (VASO) MRI are based on an endogenous contrast but they have a low sensitivity particularly at high magnetic fields, which limit their use for small animal imaging (Lu and van Zijl, 2012; Lu et al., 2003). Like CBV MRI, μDoppler imaging is particularly useful in situations in which a pure hemodynamic signal is desirable, as the more widely used BOLD signal reflects a combination of multiple variables, including CBV, CBF, $CMRO_2$ and baseline venous oxygenation. Therefore the μ-Doppler signal is easier to interpret and should reflect the "plumbing of the brain". Interestingly, we find that the temporal parameters of the CBV HRF and blood velocity measured using functional ultrasound present similar profiles than those measured using CBV fMRI (Hirano et al., 2011). For example, with comparable forepaw stimulation, this group found a 2% increase in CBV for a single impulse with a slightly longer time to peak (1 s). They also found a gradient of decreasing velocities from upper to bottom part of the cortex during functional activation. This is the first demonstration that the CBV HRF measured by functional ultrasound imaging correlates with other techniques.

Anesthesia interference with neurovascular coupling

It has been extensively demonstrated that hemodynamic coupling to neural activity is dependent on the anesthetic that can change both neuronal excitability and vascular reactivity (Masamoto and Kanno, 2012). For this reason, we decided to not pool results obtained under ketamine/xylazine (KET) anesthesia at day 0 with those obtained 2 and 7 days after the surgery under isoflurane (ISO) anesthesia. Nevertheless, we observed that TTP, FHWM and peak amplitude of the CBV HRF in the activated cortical area were not significantly different between the 2 anesthetics (data not shown). Fig. 7A presents the cortical microvasculature while Fig. 7B shows a representative correlation map obtained when stimulating the forepaw with 25 pulses under KET for the same animal. This map displays the correlation between the CBV and the stimulus pattern. Under KET, we observed a significant activation in the contralateral hemisphere but also a strong anticorrelation in the ipsilateral

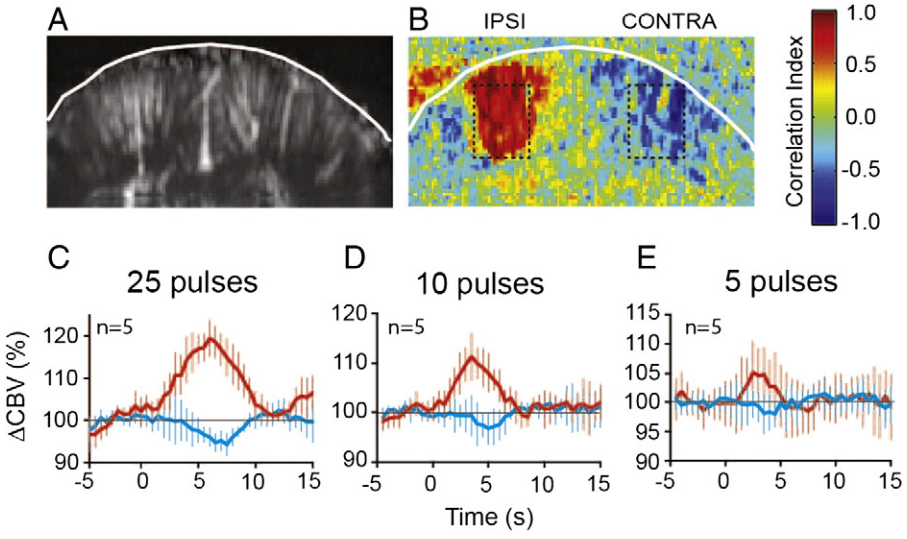

Fig. 7. Effect of ketamine/xylazine anesthesia on the HRF. (A) μDoppler image of the brain vasculature. (B) Correlation map obtained with a 25 pulse stimulus (n = 5 trials). Black lines show the two ROIs used for HRF calculation. Temporal characteristics of the CBV HRF (5 trials per curve) in response to a 25 pulse (C), a 10 pulse (D) or a 5 pulse (E) stimulation. A decrease of CBV is observed in the ipsilateral FL region.

hemisphere that was not present under ISO. This result is intriguing and may be termed as a negative CBV effect. The origin of this negative CBV response is unknown and will be the subject of further experiments. A similar effect called the negative BOLD effect has often been observed in fMRI (Schafer et al., 2012) and is presently highly debated. In future work, we would like to investigate if this negative CBV effect is correlated or not with a decrease in LFP as observed in previous fMRI studies (Shmuel et al., 2006). We hypothesize that this effect could be due to an interhemispheric inhibition that occurs via the corpus callosum (Bloom and Hynd, 2005). Although almost all callosal fibers are excitatory (van der Knaap and van der Ham, 2011), they can exert an inhibitory effect by targeting GABAergic interneurons that contain vasoactive substance (Cauli and Hamel, 2010). A reason why the negative CBV effect can only be observed under ketamine/xylazine may be due to physiological effects of ISO anesthesia on the neurotransmission with a decrease of excitatory synaptic transmission (Richards, 2002), a reduction of presynaptic excitability (Wu et al., 2004) and an enhancement of transmitter uptake in presynaptic terminals and astrocytes (Larsen et al., 1997).

We have proved that functional ultrasound imaging is a suited method to precisely quantify hemodynamic parameters in the whole rodent brain in chronic conditions. If the same quality of imaging can be achieved in freely moving animals, it would become the first method able to follow whole brain activity in behavioral experiments.

Acknowledgments

This work was supported by grants from Agence Nationale de la Recherche, Paris, France (ANR BRAINVASC). We wish to thank Claude Robert, Laurence Bourgeois and Luis Villanueva for their help with extracellular recordings.

Appendix A. Supplementary data

Supplementary data to this article can be found online at http://dx.doi.org/10.1016/j.neuroimage.2014.06.063.

References

Berwick, J., Johnston, D., Jones, M., Martindale, J., Martin, C., Kennerley, A.J., Redgrave, P., Mayhew, J.E., 2008. Fine detail of neurovascular coupling revealed by spatiotemporal analysis of the hemodynamic response to single whisker stimulation in rat barrel cortex. J. Neurophysiol. 99, 787–798.
Bloom, J.S., Hynd, G.W., 2005. The role of the corpus callosum in interhemispheric transfer of information: excitation or inhibition? Neuropsychol. Rev. 15, 59–71.
Cauli, B., Hamel, E., 2010. Revisiting the role of neurons in neurovascular coupling. Front. Neuroenerg. 2, 9.
Chen, Y., Aguirre, A.D., Ruvinskaya, L., Devor, A., Boas, D.A., Fujimoto, J.G., 2009. Optical coherence tomography (OCT) reveals depth-resolved dynamics during functional brain activation. J. Neurosci. Methods 178, 162–173.
Clement, G.T., Sun, J., Hynynen, K., 2001. The role of internal reflection in transskull phase distortion. Ultrasonics 39, 109–113.
Cole, J.T., Yarnell, A., Kean, W.S., Gold, E., Lewis, B., Ren, M., McMullen, D.C., Jacobowitz, D.M., Pollard, H.B., O'Neill, J.T., Grunberg, N.E., Dalgard, C.L., Frank, J.A., Watson, W.D., 2011. Craniotomy: true sham for traumatic brain injury, or a sham of a sham? J. Neurotrauma 28, 359–369.
Deverson, S., Evans, D.H., Bouch, D.C., 2000. The effects of temporal bone on transcranial Doppler ultrasound beam shape. Ultrasound Med. Biol. 26, 239–244.
Devor, A., Dunn, A.K., Andermann, M.L., Ulbert, I., Boas, D.A., Dale, A.M., 2003. Coupling of total hemoglobin concentration, oxygenation, and neural activity in rat somatosensory cortex. Neuron 39, 353–359.
Drew, P.J., Shih, A.Y., Driscoll, J.D., Knutsen, P.M., Blinder, P., Davalos, D., Akassoglou, K., Tsai, P.S., Kleinfeld, D., 2010. Chronic optical access through a polished and reinforced thinned skull. Nat. Methods 7, 981–984.
Hirano, Y., Stefanovic, B., Silva, A.C., 2011. Spatiotemporal evolution of the functional magnetic resonance imaging response to ultrashort stimuli. J. Neurosci. 31, 1440–1447.
Hoffmeyer, H.W., Enager, P., Thomsen, K.J., Lauritzen, M.J., 2007. Nonlinear neurovascular coupling in rat sensory cortex by activation of transcallosal fibers. J. Cereb. Blood Flow Metab. 27, 575–587.
Hu, X., Yacoub, E., 2012. The story of the initial dip in fMRI. Neuroimage 62, 1103–1108.
Hu, X., Le, T.H., Ugurbil, K., 1997. Evaluation of the early response in fMRI in individual subjects using short stimulus duration. Magn. Reson. Med. 37, 877–884.
Kim, T., Masamoto, K., Fukuda, M., Vazquez, A., Kim, S.G., 2010. Frequency-dependent neural activity, CBF, and BOLD fMRI to somatosensory stimuli in isoflurane-anesthetized rats. Neuroimage 52, 224–233.
Larsen, M., Hegstad, E., Berg-Johnsen, J., Langmoen, I.A., 1997. Isoflurane increases the uptake of glutamate in synaptosomes from rat cerebral cortex. Br. J. Anaesth. 78, 55–59.
Logothetis, N.K., Pauls, J., Augath, M., Trinath, T., Oeltermann, A., 2001. Neurophysiological investigation of the basis of the fMRI signal. Nature 412, 150–157.
Lowe, L.H., Bulas, D.I., 2005. Transcranial Doppler imaging in children: sickle cell screening and beyond. Pediatr. Radiol. 35, 54–65.
Lu, H., van Zijl, P.C., 2012. A review of the development of vascular-space-occupancy (VASO) fMRI. Neuroimage 62, 736–742.
Lu, H., Golay, X., Pekar, J.J., Van Zijl, P.C., 2003. Functional magnetic resonance imaging based on changes in vascular space occupancy. Magn. Reson. Med. 50, 263–274.
Mace, E., Montaldo, G., Cohen, I., Baulac, M., Fink, M., Tanter, M., 2011. Functional ultrasound imaging of the brain. Nat. Methods 8, 662–664.
Mace, E., Montaldo, G., Osmanski, B.F., Cohen, I., Fink, M., Tanter, M., 2013. Functional ultrasound imaging of the brain: theory and basic principles. IEEE Trans. Ultrason. Ferroelectr. Freq. Control 60, 492–506.
Malonek, D., Dirnagl, U., Lindauer, U., Yamada, K., Kanno, I., Grinvald, A., 1997. Vascular imprints of neuronal activity: relationships between the dynamics of cortical blood flow, oxygenation, and volume changes following sensory stimulation. Proc. Natl. Acad. Sci. U. S. A. 94, 14826–14831.
Masamoto, K., Kanno, I., 2012. Anesthesia and the quantitative evaluation of neurovascular coupling. J. Cereb. Blood Flow Metab. 32, 1233–1247.
Masamoto, K., Kim, T., Fukuda, M., Wang, P., Kim, S.G., 2007. Relationship between neural, vascular, and BOLD signals in isoflurane-anesthetized rat somatosensory cortex. Cereb. Cortex 17, 942–950.
Montaldo, G., Tanter, M., Bercoff, J., Benech, N., Fink, M., 2009. Coherent plane-wave compounding for very high frame rate ultrasonography and transient elastography. IEEE Trans. Ultrason. Ferroelectr. Freq. Control 56, 489–506.
Nguyen, J., Nishimura, N., Fetcho, R.N., Iadecola, C., Schaffer, C.B., 2011. Occlusion of cortical ascending venules causes blood flow decreases, reversals in flow direction, and vessel dilation in upstream capillaries. J. Cereb. Blood Flow Metab. 31, 2243–2254.
Ogawa, S., Lee, T.M., Kay, A.R., Tank, D.W., 1990. Brain magnetic resonance imaging with contrast dependent on blood oxygenation. Proc. Natl. Acad. Sci. U. S. A. 87, 9868–9872.
Paxinos, G., Watson, C., Pennisi, M., Topple, A., 1985. Bregma, lambda and the interaural midpoint in stereotaxic surgery with rats of different sex, strain and weight. J. Neurosci. Methods 13, 139–143.
Raichle, M.E., MacLeod, A.M., Snyder, A.Z., Powers, W.J., Gusnard, D.A., Shulman, G.L., 2001. A default mode of brain function. Proc. Natl. Acad. Sci. U. S. A. 98, 676–682.
Richards, C.D., 2002. Anaesthetic modulation of synaptic transmission in the mammalian CNS. Br. J. Anaesth. 89, 79–90.
Ries, F., Kaal, K., Schultheiss, R., Solymosi, L., Schlief, R., 1991. Air microbubbles as a contrast medium in transcranial Doppler sonography. A pilot study. J. Neuroimaging 1, 173–178.
Roth, T.L., Nayak, D., Atanasijevic, T., Koretsky, A.P., Latour, L.L., McGavern, D.B., 2014. Transcranial amelioration of inflammation and cell death after brain injury. Nature 505, 223–228.
Roy, C.S., Sherrington, C.S., 1890. On the regulation of the blood-supply of the brain. J. Physiol. 11 (85–158), 117.
Schafer, K., Blankenburg, F., Kupers, R., Gruner, J.M., Law, I., Lauritzen, M., Larsson, H.B., 2012. Negative BOLD signal changes in ipsilateral primary somatosensory cortex are associated with perfusion decreases and behavioral evidence for functional inhibition. Neuroimage 59, 3119–3127.
Sheth, S., Nemoto, M., Guiou, M., Walker, M., Pouratian, N., Toga, A.W., 2003. Evaluation of coupling between optical intrinsic signals and neuronal activity in rat somatosensory cortex. Neuroimage 19, 884–894.
Shih, A.Y., Driscoll, J.D., Drew, P.J., Nishimura, N., Schaffer, C.B., Kleinfeld, D., 2012. Two-photon microscopy as a tool to study blood flow and neurovascular coupling in the rodent brain. J. Cereb. Blood Flow Metab. 32, 1277–1309.
Shmuel, A., Augath, M., Oeltermann, A., Logothetis, N.K., 2006. Negative functional MRI response correlates with decreases in neuronal activity in monkey visual area V1. Nat. Neurosci. 9, 569–577.
Shung, K.K., Sigelmann, R.A., Reid, J.M., 1976. Scattering of ultrasound by blood. IEEE Trans. Biomed. Eng. 23, 460–467.
Silva, A.C., Koretsky, A.P., Duyn, J.H., 2007. Functional MRI impulse response for BOLD and CBV contrast in rat somatosensory cortex. Magn. Reson. Med. 57, 1110–1118.
Sloan, M.A., Alexandrov, A.V., Tegeler, C.H., Spencer, M.P., Caplan, L.R., Feldmann, E., Wechsler, L.R., Newell, D.W., Gomez, C.R., Babikian, V.L., Lefkowitz, D., Goldman, R.S., Armon, C., Hsu, C.Y., Goodin, D.S., Therapeutics, Technology Assessment Subcommittee of the American Academy of, N, 2004. Assessment: transcranial Doppler ultrasonography: report of the Therapeutics and Technology Assessment Subcommittee of the American Academy of Neurology. Neurology 62, 1468–1481.
Srinivasan, V.J., Sakadzic, S., Gorczynska, I., Ruvinskaya, S., Wu, W., Fujimoto, J.G., Boas, D.A., 2010. Quantitative cerebral blood flow with optical coherence tomography. Opt. Express 18, 2477–2494.
Van Camp, N., Verhoye, M., Van der Linden, A., 2006. Stimulation of the rat somatosensory cortex at different frequencies and pulse widths. NMR Biomed. 19, 10–17.
van der Knaap, L.J., van der Ham, I.J., 2011. How does the corpus callosum mediate interhemispheric transfer? A review. Behav. Brain Res. 223, 211–221.
van Raaij, M.E., Lindvere, L., Dorr, A., He, J., Sahota, B., Foster, F.S., Stefanovic, B., 2011. Functional micro-ultrasound imaging of rodent cerebral hemodynamics. Neuroimage 58, 100–108.
Woolsey, T.A., Rovainen, C.M., Cox, S.B., Henegar, M.H., Liang, G.E., Liu, D., Moskalenko, Y.E., Sui, J., Wei, L., 1996. Neuronal units linked to microvascular modules in cerebral cortex: response elements for imaging the brain. Cereb. Cortex 6, 647–660.
Wu, X.S., Sun, J.Y., Evers, A.S., Crowder, M., Wu, L.G., 2004. Isoflurane inhibits transmitter release and the presynaptic action potential. Anesthesiology 100, 663–670.
Xiang, L., Ji, L., Zhang, T., Wang, B., Yang, J., Zhang, Q., Jiang, M.S., Zhou, J., Carney, P.R., Jiang, H., 2012. Noninvasive real time tomographic imaging of epileptic foci and networks. Neuroimage 66C, 240–248.

Xu, H.T., Pan, F., Yang, G., Gan, W.B., 2007. Choice of cranial window type for in vivo imaging affects dendritic spine turnover in the cortex. Nat. Neurosci. 10, 549–551.

Yiu, B.Y., Tsang, I.K., Yu, A.C., 2011. GPU-based beamformer: fast realization of plane wave compounding and synthetic aperture imaging. IEEE Trans. Ultrason. Ferroelectr. Freq. Control 58, 1698–1705.

Yu, X., Wang, S., Chen, D.Y., Dodd, S., Goloshevsky, A., Koretsky, A.P., 2010. 3D mapping of somatotopic reorganization with small animal functional MRI. Neuroimage 49, 1667–1676.

Yu, X., Glen, D., Wang, S., Dodd, S., Hirano, Y., Saad, Z., Reynolds, R., Silva, A.C., Koretsky, A. P., 2012. Direct imaging of macrovascular and microvascular contributions to BOLD fMRI in layers IV–V of the rat whisker-barrel cortex. Neuroimage 59, 1451–1460.